

Ionization memory of plasma emitters in a solar prominence

E. Wiehr^{1,*}, H. Balthasar², G. Stellmacher³, and M. Bianda⁴

¹ Institut für Astrophysik, Universität Göttingen, Friedrich-Hund-Platz 1, 37077 Göttingen, Germany

² Leibniz-Institut für Astrophysik Potsdam (AIP), An der Sternwarte 16, 14482 Potsdam, Germany
e-mail: hbalthasar@aip.de

³ Institute d'Astrophysique, 98 bis Boulevard Arago, 75014 Paris, France

⁴ Istituto ricerche solari Aldo e Cele Daccó (IRSOL), Università della Svizzera italiana, Via Patocchi 57, 6605 Locarno-Monti, Switzerland

Received July 16, 2024; accepted March 07, 2025

ABSTRACT

Context.

Aims. In the low-collisional, partially ionized plasma (PIP) of solar prominences, uncharged emitters might show different signatures of magnetic line broadening than charged emitters. We investigate if the widths of weak metal emissions in prominences exceed the thermal line broadening by a different amount for charged and for uncharged emitters.

Methods. We simultaneously observe five optically thin, weak metal lines in the brightness center of a quiescent prominence and compare their observed widths with the thermal broadening.

Results. The inferred non-thermal broadening of the metal lines does not indicate systematic differences between the uncharged Mg b₂ and Na D₁ and the charged Fe II emitters, only Sr II is broader.

Conclusions. The additional line broadening of charged emitters is reasonably attributed to magnetic forces. That of uncharged emitters can then come from their temporary state as ion before recombination. Magnetically induced velocities will retain some time after recombination. Modelling partially ionized plasmas then requires consideration of a memory of previous ionization states.

Key words. Sun: filaments, prominences – Techniques: spectroscopic – Methods: observational

1. Introduction

The study of partially ionized plasmas (PIP) has become increasingly important in recent years (Khomenko 2017; Ballester et al. 2018; Soler & Ballester 2022; Parenti et al. 2024; Heinzl et al. 2024). A reduced collisional rate of the PIP enables a decoupling of charged and uncharged species which leads to different dynamical behavior of them. Higher flow velocities (line shifts) of ions are observed by Khomenko et al. (2016); Wiehr et al. (2019, 2021); Zapiór et al. (2022) in solar prominences, which are ideal objects to observe such effects with high spatial and temporal resolution. Drifts of ions relative to neutrals pose a particular problem for prominence support against gravity by magnetic forces since neutrals will sink through the magnetic structure if they are not in collisional equilibrium with charged particles. Gilbert et al. (2002, 2007) report a depletion of helium in the high parts of filaments. For prominences, we expect a certain coupling between the two, but weak enough to allow drifts between ions and neutrals.

The decoupling of charged and uncharged species in a PIP can also manifest itself in a different line broadening. Already Landman (1981) expects lines from ions to be broader than such from neutrals. Ramelli et al. (2012) find for a quiescent prominence a He II line 1.5 times broader than a He I line from the triplet system which, in turn, is 1.1 times broader than a He I line from the singlet system. Stellmacher & Wiehr (2015) find that the Mg b₂ line is 1.3 times broader than the ('forbidden') intercombination line from the magnesium triplet to the singlet sys-

tem. Stellmacher & Wiehr (2017) find a width excess of Sr II and Fe II lines relative to Na D and, respectively, He-singlet, which they interpret by influences of magnetic forces. González Manrique et al. (2024) observe the Ca II 8542 Å line broader than expected from He D₃ and H α . Since strong ('chromospheric') lines such as Ca II 8542 Å and H α are optically thick in most parts of a prominence, the result is limited to the boundary between prominence and the corona where 'instabilities may take place... helping to increase the differential ion-neutral behavior...' (González Manrique et al. 2024). Pontin et al. (2020) investigate for coronal loops such line broadening in terms of magnetic 'braiding induced turbulence', but it is not fully clear if such an effect also applies in prominences.

Parenti et al. (2024) resume that 'we need the measurement of several spectral profiles from neutrals and low ionization state species under optical thin condition'. This is the aim of the present study. We observe weak metal lines which are optically thin throughout the whole prominence allowing to analyze the line broadening in the central prominence body. Such weak metal lines are rarely observed in prominences; they are mostly drowned in the parasitic light of the aureole and therefore require careful correction compared to bright 'chromospheric' lines.

2. Observations and data reduction

We improve previous sequential measurements by simultaneous observations of seven emission lines in a prominence using the THEMIS telescope on Tenerife and its echelle spectrograph. The prominence at the west limb, 52°N, on June 6, 2022 showed

* Deceased on 03 February 2025

negligible evolutionary variation (according to images from the GONG data archive) and can thus be considered as quiescent. Since slit-jaw images were not available, we reconstruct the slit positions in a prominence image from the GONG survey using the observed distribution of the H γ intensity along each slit position (Fig. 1).

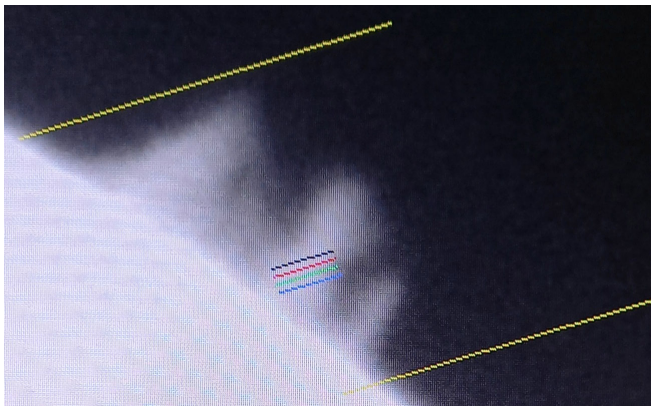


Fig. 1. H α image of the prominence at the west limb, 52° north, from June 6, 2022, (GONG archive); north direction is upwards; the long lines mark the direction of refraction at two slit positions aside the prominence used for the determination of parasitic light; the short lines mark slit positions reconstructed from the observed H γ intensity variation, their extension of 12'' corresponds to 8.7 Mm.

Given the different wavelengths of the observed lines, the spectrograph slit is reasonably aligned along the direction of refraction which varies throughout the day. Therefore, a spectrograph slit constantly oriented along the direction of refraction will rotate over the prominence. Near solstice, however, its direction remains almost constant for a few hours (see Wiehr et al. 2019). We observe from 9:06 to 9:24 UT and accordingly keep the slit at an angle of 72° clockwise from north, its width corresponding to 1'5 (≈ 1000 km on the Sun). Five cameras recorded the emission lines H γ , Na D₁, Sr II 4216 Å, and the neighboring lines He I 5015 Å and Fe II 5018 Å, and Fe II 5169 Å and Mg b₂ 5172 Å. These lines are chosen to cover an appropriate range of optically thin metal emissions from ions and neutrals that matches the grating orders.

We observe a He-singlet line to avoid correction for overlapping triplet components and prefer the slightly weaker Na D₁ line since D₂ has a terrestrial H₂O blend which does not disappear with the aureole subtraction (see Wiehr et al. 2019). Sr II 4216 Å replaces the formerly used Sr II 4078 Å to fit the grating orders, besides, it avoids possible blending with Cr II and Ce II lines. H γ is a suitable Balmer line of moderate optical thickness (Gouttebroze et al. 1993) even in bright prominences required to detect weak metall lines. Characteristics of the lines are given in Table 1.

We choose four slit positions in the prominence (see Fig. 1) with a spacing of 2''. The exposure time at each position is 2 s. We repeat the scanning over the four slit positions 50 times. The total cadence spans 20 s (exposure plus moving to the new position).

In a time interval of optimal seeing we average five time steps (no. 21 ± 2) corresponding to an effective exposure of 10 s. Since the line widths do not vary significantly over the 50 scans, we apply a running mean over nine camera rows corresponding to an effective spatial resolution of 2'16 (≈ 1500 km in the prominence; spatial scale 0'24/pixel). Disk center spectra

are taken for a calibration of the line intensities, using the continuum values by Neckel and Labs (1984). The telescope was moved around disk center to average solar structures and allow a determination of the flat field matrix.

Spectra from the immediate prominence vicinity (long lines in Fig. 1) are taken to determine the parasitic light superposed on the emission lines. In contrast to strong chromospheric emissions, the metall lines observed here are so weak that their emissions are almost lost in the aureole light and thus invisible in the raw prominence spectra. Therefore, a particularly careful correction is required to ensure that no residues of the aureole spectrum remain in the final corrected prominence spectra. This procedure is described in detail by Ramelli et al. (2012).

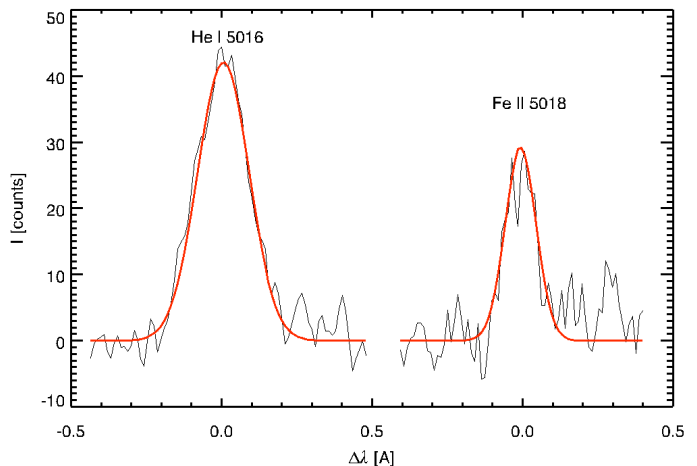


Fig. 2. Observed line profiles of He-singlet 5016 Å and Fe II 5018 Å together with the Gaussian fits. Between both lines, ≈ 2 Å are cut out to stretch the λ scale.

The weak metall lines are well represented by fitted Gaussian profiles (Fig. 2). They are corrected for the spectrograph profile to finally obtain the width of each emission line with an accuracy of ± 3 mÅ. This is approximately $\pm 3.5\%$ of the width of the metall lines, $\pm 2.5\%$ of He and $\pm 1.5\%$ of H γ . Integration of the Gaussian profiles over lambda yields the total line emission, E^{tot} , which we consider significant when that of the H γ line amounts $E_{\gamma}^{\text{tot}} > 0.4 E_{\text{max}}^{\text{tot}}$ and that of the other emission lines $E^{\text{tot}} > 0.75 E_{\text{max}}^{\text{tot}}$, where $E_{\text{max}}^{\text{tot}}$ is the brightness maximum along the slit for each emission line.

3. Results

The mean value of the total emission of H γ observed at the four slit positions amounts to $E_{\gamma}^{\text{tot}} = 4 \cdot 10^4$ erg (s cm² ster)⁻¹, for which Gouttebroze et al. (1993) give $\tau_{\gamma} = 0.5$, $\tau_{\alpha} = 10.1$ and $E_{\alpha}^{\text{tot}} = 39.6 \cdot 10^4$ erg (s cm² ster)⁻¹ (table for $T_{\text{kin}} = 8000$ K, $P = 0.2$ dyn cm⁻² and $\Delta z = 5000$ km). Such a high Balmer brightness is a necessary condition to observe weak optically thin metall lines with sufficient accuracy. Since the total emissions of the metall lines are 60 - 200 times weaker than that of H γ they can well be assumed to be optically thin. Indeed, Landman (1981) obtains for $E_{\text{max}}^{\text{tot}}(\text{Na D}_1) = 4420$ erg (s cm² ster)⁻¹ an optical thickness of $\tau_{\text{D}} = 0.1$. Our Na D₁ emission is 8 times weaker and thus $\tau_{\text{D}} < 0.1$.

The broadening of optically thin lines is usually described by a thermal and a non-thermal term, $V_{\text{obs}}^2 = V_{\text{th}}^2 + V_{\text{nth}}^2$, where V denotes the line widths $\Delta\lambda_{\text{w}}$ in velocity units: $c \cdot \Delta\lambda_{\text{w}} \lambda_0^{-1}$ (c velocity of light, λ_0 line wavelength, $\Delta\lambda_{\text{w}} = \sqrt{2}\sigma$ the half width at

| Emitter | μ^{-1} | λ [Å] | χ_{ion}^1 [eV] | χ_{ion}^2 [eV] | t_{em} [ns] | mean E^{tot} [erg (cm ² s ster) ⁻¹] | mean $\Delta\lambda \lambda^{-1}$ [10 ⁻⁵] | V_{nth} [km s ⁻¹] |
|---------------------|------------|------------------|-------------------------------|-------------------------------|------------------|--|--|---|
| Sr II | 0.0114 | 4215.52 | 5.7 | 11.0 | 7.1 | 600 | 1.9 | 5.4 |
| Fe II | 0.0179 | 5018.44 | 7.9 | 16.2 | 500.0 | 200 | 1.4 | 3.8 |
| Fe II | 0.0179 | 5169.03 | 7.9 | 16.2 | 238.1 | 350 | 1.6 | 4.4 |
| Mg I b ₂ | 0.0411 | 5172.68 | 7.6 | 15.0 | 29.7 | 720 | 1.7 | 4.4 |
| Na I D ₁ | 0.0435 | 5895.92 | 5.1 | 47.3 | 16.3 | 550 | 1.6 | 4.2 |
| He I singl. | 0.25 | 5015.68 | 24.6 | 54.4 | 74.6 | 330 | 2.4 | 3.8 |
| H 1 γ | 1.0 | 4340.72 | 13.6 | - | 395.3 | 40,000 | 4.6 | 4.5 |

Table 1. Line characteristics and data (means of the 4 slit positions). The mean emission times t_{em} are obtained as reciprocal values of the transition probabilities taken from Kramida et al. (2018).

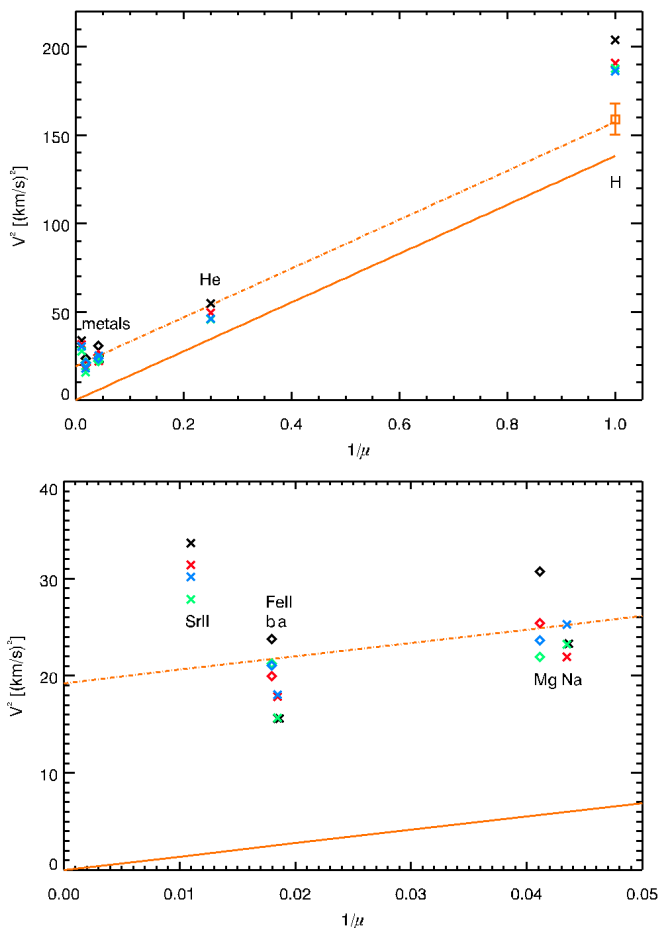


Fig. 3. Upper panel: observed mean values $V^2 = (c \cdot \Delta\lambda_w / \lambda_0)^2$ versus the inverse atomic mass $1/\mu$ for the 4 slit positions marked in Fig. 1. The dotted orange line represents a linear fit through all lines, and the solid orange line is used as reference for width excesses of the spectral lines. Diamonds for Fe II(b) and Mg b separate the close Fe II(a) and Na D values. The orange bar indicates the uncertainty of the opacity broadening of H γ . Lower panel: enlargement of the range of the metall lines. The position of Fe II(a) is slightly shifted to separate it from Fe II(b).

$I_0 e^{-1}$ with σ being the width parameter of the Gaussian fits, see Tandberg-Hanssen 1995). We determine the non-thermal term as difference $V_{\text{nth}}^2 = V_{\text{obs}}^2 - V_{\text{th}}^2$.

In Fig. 3 we plot the mean of the observed quantity $V^2 = (c \cdot \Delta\lambda_w \lambda_0^{-1})^2$ for the four slit positions versus the inverse atomic mass μ^{-1} . To obtain a reference, we calculate a linear fit through all lines using the mean values over the scan positions. The corresponding line is displayed in Fig. 3 in dashed orange. From this

fit, we subtract the value at $\mu^{-1} = 0$ and obtain the solid orange line which we use as reference for the non-thermal broadening. This line represents the pure thermal dependence for 8300 K. With respect to this reference, the line widths of metals significantly deviate. We find for Sr II, Fe II, and Mg b₂ rather similar non-thermal widths as Ramelli et al. (2012). However, we obtain significant V_{nth} for Na D₁, which those authors did not find for Na D₂. We attribute this discrepancy to the terrestrial H₂O blend in the Na D₂ wing which diminishes the line width (see Wiehr et al. 2019). H γ and He I also appear above the reference line. For H γ one has to take into account an additional broadening due to opacity, which we estimate from the tables by Gouttebroze et al. (1993) for 8000 K to be $(10 \pm 3)\%$. The reduced V is given by the orange bar in Fig. 3.

In Fig. 4 we plot for the metall lines the deviations of the observed widths from the reference line in Fig. 3 in velocity units $c \cdot \Delta\lambda_w \lambda_0^{-1}$ versus the inverse atomic mass μ^{-1} (as in Fig. 3) and find a range of $3.5 < V_{\text{nth}} < 6.0$ km s⁻¹. Mean values are listed in the last column of Tab. 1.

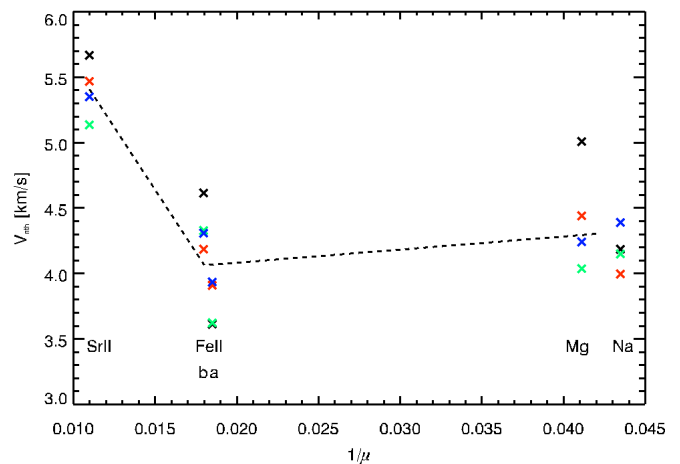


Fig. 4. Deviation of the observed widths of metall lines from the reference line in Fig. 3 in velocity units $c \cdot \Delta\lambda_w \lambda_0^{-1}$ [km/s]. Values for the 4 slit positions appear in the same colors as in Fig. 1. Fe II(a) 5018 Å is shifted by $\Delta 1/\mu = 0.005$ to separate from Fe II(b) 5169 Å.

4. Discussion and Conclusions

The non-thermal line broadening reflects small-scale motions which, in contrast to line shift data, are independent of the line-of-sight angle and supposed to result from interaction with the magnetic field (Parenti et al. 2024). The observation of weak metall lines allows to study the bright prominence body without

| Emitter | l_{fp} | $t_c(v=2 \text{ km s}^{-1})$ | $t_c(v=4 \text{ km s}^{-1})$ | $t_c(v=6 \text{ km s}^{-1})$ | $t_c(v=8 \text{ km s}^{-1})$ | $t_c(v=10 \text{ km s}^{-1})$ |
|---------------------|----------|------------------------------|------------------------------|------------------------------|------------------------------|-------------------------------|
| Sr II | 11.4 m | 5.7 ms | 2.8 ms | 1.9 ms | 1.4 ms | 1.1 ms |
| Fe II | 25.2 m | 12.6 ms | 6.3 ms | 4.2 ms | 3.2 ms | 2.5 ms |
| Mg I b ₂ | 10.9 m | 5.4 ms | 2.7 ms | 1.8 ms | 1.3 ms | 1.1 ms |
| Na I D ₁ | 7.2 m | 3.6 ms | 1.8 ms | 1.2 ms | 0.9 ms | 0.7 ms |
| He I singl. | 60.4 m | 30.2 ms | 15.1 ms | 10.0 ms | 7.6 ms | 6.0 ms |
| H I γ | 37.9 m | 19.0 ms | 9.5 ms | 6.3 ms | 4.7 ms | 3.8 ms |

Table 2. Free path lengths and mean collision times for the different ions assuming the hydrogen density from the table for $T_{kin} = 8000 \text{ K}$ and $p = 0.2 \text{ dyn cm}^{-2}$ by Gouttebroze et al. (1993).

influences of optical thickness. The finally obtained line width excesses are thus not restricted to the prominence border as for strong chromospheric lines. Our lines, however, are too weak for a study of the periphery but give sufficient signal only at the bright prominence center.

The most prominent result of our study is the almost equal broadening excess of lines from ionized Fe and neutral Na and Mg. For Mg b₂ this result confirms the findings by Ramelli et al. (2012) who argue that triplet systems are populated via ionization and recombination. During the intermediate state as ion magnetic influences modify the velocity distribution. We interpret the broadening of neutral metals by a kind of ‘ionization memory’ occurring after recombination if the line emission happens before a collision changes the momentum of the atom. To get an idea about collision times in the prominence plasma, we use the equation for the length of the free path length

$$l_{fp} = (4\pi\sqrt{2})^{-1}n^{-1}r^{-2},$$

where n is the particle density and r the mean radius of the colliding atoms (Gerthsen & Kneser 1971, p. 64). The particle density of hydrogen is taken from Gouttebroze et al. (1993) for parameters $T=8000 \text{ K}$, $p=0.2 \text{ dyn cm}^{-2}$, $\Delta z = 5000 \text{ km}$ which fit our observed E_{γ}^{tot} (see Tab. 1) Atomic radii are given by Clementi et al. (1967), and we take ionic radii from www.webelements.com. These values concern the ground state, but since emitting atoms are excited, we enlarge radii by a factor of two as coarse estimate. We consider collisions of the investigated metals with neutral hydrogen and helium and neglect all other species because they are less frequent, and protons are much smaller, thus they contribute only little. Dividing this length by the typical velocity of the colliding particles, we obtain the mean collision time t_c . Such velocities vary between 4 and 10 km s^{-1} for metals (see Fig. 3), resulting in $10^{-3} \text{ s} < t_c < 10^{-1} \text{ s}$. A detailed overview is given in Table 2. The widths of metall lines indicate that each emitter has its individual broadening sensitivity, depending on the time interval between recombination and line emission. The neutral metals apparently have a memory of their previous period as ions and maintain their velocity distribution after recombination. This becomes plausible comparing the mean emission time after recombination ($10^{-9} - 10^{-6} \text{ s}$; see 1) and the mean collision time ($10^{-4} - 10^{-1} \text{ s}$). Although the collision times are approximative, the differences of a few orders of magnitude to the emission times justifies our suggestion of an ‘ionization memory’.

Concerning the large line broadening excess of Na D₁ (not observed by Ramelli et al., 2012), Landman (1981, 1983) argues that sodium is mostly ionized (see ionization potentials in Tab. 1). Short time after recombination the D lines are emitted. The mean time span between recombination and emission is given in Tab. 1. So, magnetic forces had influenced sodium during its previous existence as ion.

The highest broadening excess is found for Sr II in agreement with Ramelli et al. (2012). Strontium may be particularly

sensible to magnetic influences since it exists, according to the low second ionization potential in Tab. 1, most of the time as Sr III (see Landman 1983). [We note that the Sr II line widths are not affected by isotopy shifts which, according to Heilig (1961), amount to about 1 m\AA .]

Ions experience in the magnetic field the Lorentz force, according to the equation

$$F = kqv \times B,$$

where q is the electric charge, B the magnetic field, v the velocity, and k is a prefactor. The Lorentz force causes a gyration of an ion around the magnetic fieldlines with the speed of the component of v perpendicular to the magnetic field, but not a linear acceleration of the ion. In the corresponding plane, all directions occur, and in the consequence we observe a broadening of the spectral lines (see also Ballester et al. 2018). Another broadening effect arises when the velocity component along the magnetic field is non-zero and the magnetic field is not everywhere perpendicular to gravity direction, e. g. in the magnetic field configuration suggested by Kippenhahn & Schlüter (1957). Then a pendular motion of the ion around the local height minimum of the field lines can occur causing a broadening of the emission lines. Different types of waves also influence the line broadening as well as instabilities or shocks and motions in twisted flux tubes. Such effects are discussed in detail by Ballester et al. (2018). Prominences typically consist of thin threads which are not resolved in our data due to our long exposure times. These threads can move against each other causing a line broadening.

The observed fact that lines from metall emitters are broader than expected from our reference line (see Fig. 3) suggests that the metall emissions are broadened by non-thermal effects. The observed mean Sr II line width would require unlikely high $T_{kin} = 175,000 \text{ K}$ if only thermally broadened. Since the observed line profiles are almost perfect Gaussians, we can assume a Maxwellian distribution of non-thermal motions. The helium line also is broader than our reference line indicating a non-thermal broadening. This can be due to collisions on a longer time scale than the mean emission time. Because of the high ionization potential, only a small fraction of helium atoms will be ionized (see Labrosse & Gouttebroze 2001). The excitation of the helium singlet system is then caused mainly by absorption of EUV radiation ($\lambda\lambda 584 \text{ \AA}$ and 537 \AA) from the chromosphere, in the first case then emission of a $2 \mu\text{m}$ photon and absorption of a photospheric photon ($\lambda\lambda 5016 \text{ \AA}$). In contrast, for the triplet system, photo-ionization and recombination play an important role.

Detailed physical processes behind such non-thermal broadening remain still unclear. They are assumed to be of magnetic origin (Parenti et al. 2024). Instabilities at the prominence-corona border can be excluded because our data refer exclusively to the prominence bulge. Since lines from neutral emitters seem to be broadened according to their intermediate existence as ion,

a description by a dual scenario 'charged-uncharged' will not be sufficient.

Acknowledgements. We are indebted to M. Verma for carefully reading and commenting the manuscript. We thank B. Gelly and D. Laforgue for assistance with the instrument. THEMIS is operated by CNRS-INSU in the Spanish Observatorio del Teide, Tenerife. E.W. and H.B. received financial support from the European Union's Horizon 2020 research and innovation program under grant agreement No. 824135 (SOLARNET).

References

- Ballester, J. L., Alexeev, I., Collados, M., et al. 2018, *Space Sci. Rev.*, 214, 58
- Clementi, E., Raimondi, D. L., & Reinhardt, W. P. 1967, *J. Chem. Phys.*, 47, 1300
- Gerthsen, C. & Kneser, H. O. 1971, *Physik. Elfte berichtigte Auflage* (Springer Verlag Berlin Heidelberg New York)
- Gilbert, H., Kilper, G., & Alexander, D. 2007, *ApJ*, 671, 978
- Gilbert, H. R., Hansteen, V. H., & Holzer, T. E. 2002, *ApJ*, 577, 464
- González Manrique, S. J., Khomenko, E., Collados, M., et al. 2024, *A&A*, 681, A114
- Gouttebroze, P., Heinzel, P., & Vial, J. C. 1993, *A&AS*, 99, 513
- Heilig, K. 1961, *Zeitschrift für Physik*, 161, 252
- Heinzel, P., Gunár, S., & Ježić, S. 2024, *Philosophical Transactions of the Royal Society of London Series A*, 382, 20230221
- Khomenko, E. 2017, *Plasma Physics and Controlled Fusion*, 59, 014038
- Khomenko, E., Collados, M., & Díaz, A. J. 2016, *ApJ*, 823, 132
- Kippenhahn, R. & Schlüter, A. 1957, *ZAp*, 43, 36
- Kramida, A., Ralchenko, Y., Nave, G., & Reader, J. 2018, in *APS Meeting Abstracts*, Vol. 2018, APS Division of Atomic, Molecular and Optical Physics Meeting Abstracts, M01.004
- Labrosse, N. & Gouttebroze, P. 2001, *A&A*, 380, 323
- Landman, D. A. 1981, *ApJ*, 251, 768
- Landman, D. A. 1983, *ApJ*, 269, 728
- Parenti, S., Luna, M., & Ballester, J. L. 2024, *Philosophical Transactions of the Royal Society of London Series A*, 382, 20230225
- Pontin, D. I., Peter, H., & Chitta, L. P. 2020, *A&A*, 639, A21
- Ramelli, R., Stellmacher, G., Wiehr, E., & Bianda, M. 2012, *Sol. Phys.*, 281, 697
- Soler, R. & Ballester, J. L. 2022, *Frontiers in Astronomy and Space Sciences*, 9, 789083
- Stellmacher, G. & Wiehr, E. 2015, *A&A*, 581, A141
- Stellmacher, G. & Wiehr, E. 2017, *Sol. Phys.*, 292, 83
- Tandberg-Hanssen, E. 1995, *Astrophysics and Space Science Library*, Vol. 199, The nature of solar prominences (Kluwer Academic Publishers, Dordrecht)
- Wiehr, E., Stellmacher, G., Balthasar, H., & Bianda, M. 2021, *ApJ*, 920, 47
- Wiehr, E., Stellmacher, G., & Bianda, M. 2019, *ApJ*, 873, 125
- Zapiór, M., Heinzel, P., & Khomenko, E. 2022, *ApJ*, 934, 16